

Electronic structure of quantum spheres with wurtzite structure

Jian-Bai Xia and Jingbo Li

China Center for Advanced Science and Technology (World Laboratory), P.O. Box 8730, Beijing 100080, People's Republic of China
and National Laboratory for Superlattices and Microstructures, Institute of Semiconductors, Chinese Academy of Sciences,
P.O. Box 912, Beijing 100083, People's Republic of China

(Received 4 June 1999)

The hole effective-mass Hamiltonian for the semiconductors with wurtzite structure is given. The effective-mass parameters are determined by fitting the valence-band structure near the top with that calculated by the empirical pseudopotential method. The energies and corresponding wave functions are calculated with the obtained effective-mass Hamiltonian for the CdSe quantum spheres, and the energies as functions of sphere radius R are given for the zero spin-orbital coupling (SOC) and finite SOC cases. The energies do not vary as $1/R^2$ as the general cases, which is caused by the crystal-field splitting energy and the linear terms in the Hamiltonian. It is found that the ground state is not the optically active S state for the R smaller than 30 Å, in agreement with the experimental results and the "dark exciton" theory. [S0163-1829(99)01040-1]

I. INTRODUCTION

Semiconductor nanocrystals offer the opportunity to explore the evolution of electronic and optical properties as the size of the system decreases from bulk to the nanometer scale. In addition, their strongly size-dependent optical properties render them attractive candidates as tunable light absorbers and emitters in optoelectronic devices. New fabrication methods have enabled the synthesis of highly monodisperse ($\sigma_R < 4\%$) CdSe nanocrystals with radii tunable between 10 and 50 Å, which have a luminescence with high quantum yield (10–15% at 10 K).¹ Recently, Hines *et al.*² have reported making core-shell (CdSe)ZnS nanocrystallites that photoluminesce with a quantum yield of 50% at 530 nm. Mikulec *et al.*³ synthesized high quantum yield (30–50%) core-shell (CdSe)ZnS nanocrystallites of various sizes with narrow band edge luminescence spanning most of the visible spectrum from 470 nm to 625 nm. Empedocles *et al.*⁴ used far-field microscopy to image and obtain ultranarrow single dot luminescence (SDL) spectra from single CdSe nanocrystallites at 10 K. The elimination of spectral inhomogeneities reveals new spectral phenomena including light driven spectral diffusion, which is consistent with a Stark effect.

The Stark effect of the quantum dots and the electronic states of the overcoated quantum dots (quantum-dot quantum-well structures) have been investigated by Chang and Xia^{5,6} for those with zinc-blende structure in the framework of the effective-mass envelope-function theory.⁷ For CdS, CdSe, and ZnS nanocrystallites the common lattice structure is hexagonal (wurtzite), which was proved by high-resolution TEM and x-ray diffraction.¹ Efros *et al.*⁸ considered the crystal shape asymmetry and the intrinsic crystal field (hexagonal) within the framework of a quasicubic model, and obtained optically passive (dark exciton) and optically active (bright exciton) states for CdSe quantum dots. The theoretical results are in agreement with the size dependence of Stokes shifts obtained in fluorescence line narrowing and photoluminescence experiments for CdSe nanocrystals.

In this paper we shall study the electronic states of quantum dots with wurtzite lattice structure from their hole effective-mass Hamiltonian. Chung *et al.*⁹ derived the effective-mass Hamiltonian for wurtzite semiconductors, but not including the p linear terms, which have been proved to be essential for the energy bands near the valence-band top. We derived the correct effective-mass Hamiltonian for wurtzite semiconductors including the p linear terms,¹⁰ and shall use this Hamiltonian as the basis of the present study. A spherical quantum dot with a finite potential barrier was studied in our previous paper.⁶ For simplicity, in this paper we assume that the quantum sphere is surrounded by an infinitely high potential barrier represented by the matrix material, but the finite potential barrier can be taken into account conveniently in our method. The remainder of the paper is organized as follows. In Sec. II we introduce a model of the system being considered and present the calculation method. Our numerical results and discussions are given in Sec. III. Finally, we draw a brief conclusion in Sec. IV.

II. MODEL AND CALCULATION

The hole effective-mass Hamiltonian for wurtzite semiconductors was derived in Ref. 10 for the case of zero spin-orbital coupling (SOC),

TABLE I. Fitting parameters of CdS, CdSe, and ZnS atomic pseudopotentials.

| | v_1 | v_2 | v_3 | v_4 |
|-----|--------|--------|--------|--------|
| Cd | 0.0564 | 1.0287 | 1.2920 | 3.8489 |
| S | 0.3297 | 2.5053 | 1.6005 | 1.7289 |
| Cd | 0.1067 | 1.4241 | 1.3132 | 3.1482 |
| Se | 0.1744 | 3.0802 | 1.7910 | 2.6251 |
| ZnS | 0.0536 | 1.2390 | 0.9270 | 4.3598 |
| S | 0.2337 | 3.1110 | 1.3657 | 3.1969 |

$$H = \frac{1}{2m_0} \begin{vmatrix} Lp_x^2 + Mp_y^2 + Np_z^2 & Rp_xp_y & Ap_0p_x + Qp_xp_z \\ Rp_xp_y & Lp_y^2 + Mp_x^2 + Np_z^2 & Ap_0p_y + Qp_y p_z \\ Ap_0p_x + Qp_xp_z & Ap_0p_y + Qp_y p_z & S(p_x^2 + p_y^2) + Tp_z^2 + 2m_0\Delta_c \end{vmatrix}, \quad (1)$$

where the basic functions are X-like, Y-like (Γ_6), and Z-like (Γ_1) functions, respectively, L, M, \dots, S, T are effective-mass parameters, and Δ_c is the crystal-field splitting energy. For the II-VI compounds such as CdS, ZnS, and CdSe, the Γ_6 energy levels of the valence band are higher than the Γ_1 energy level, so Δ_c is greater than zero [hereafter we take the negative hole energy as positive, as shown in Eq. (1)]. The effective-mass parameters are determined by fitting the energy bands near the valence-band top with those calculated by the empirical pseudopotential method as in Ref. 10. The form factors of the atomic pseudopotentials are fitted with Cohen's formula,¹¹

$$V(G) = \frac{v_1(G^2 - v_2)}{e^{v_3(G^2 - v_4) + 1}}, \quad (2)$$

where v_1, v_2, v_3 , and v_4 are empirical parameters determined by the experimental energy values or *ab initio* theoretical calculation values at some special points of the Brillouin zone.

Table I gives the fitted $v_1 - v_4$ values for the CdS, CdSe, and ZnS atomic pseudopotentials, where the unit of G is a.u.⁻¹. At the same time, the effective-mass parameters of hexagonal semiconductors are listed in Table II for CdS, CdSe, and ZnS material, respectively.

Transforming the basic functions X, Y , and Z into $|11\rangle = 1/\sqrt{2}(X + iY)$, $|10\rangle = Z$, and $|1-1\rangle = 1/\sqrt{2}(X - iY)$, the hole Hamiltonian (1) can be written as

$$H = \frac{1}{2m_0} \begin{vmatrix} P_1 & S & T \\ S^* & P_3 & S \\ T^* & S^* & P_1 \end{vmatrix}, \quad (3)$$

where

$$\begin{aligned} P_1 &= \gamma_1 p^2 - \sqrt{\frac{2}{3}} \gamma_2 P_0^{(2)}, \\ P_3 &= \gamma_1' p^2 + 2 \sqrt{\frac{2}{3}} \gamma_2' P_0^{(2)} + 2m_0 \Delta_c, \\ T &= \eta P_{-2}^{(2)} + \delta P_2^{(2)}, \end{aligned} \quad (4)$$

$$T^* = \eta P_2^{(2)} + \delta P_{-2}^{(2)},$$

$$S = Ap_0 P_{-1}^{(1)} + \sqrt{2} \gamma_3' P_{-1}^{(2)},$$

$$S^* = -Ap_0 P_1^{(2)} - \sqrt{2} \gamma_3' P_1^{(2)}.$$

$P^{(2)}, P^{(1)}$ are the second-order and first-order tensors of the momentum operator, respectively. The effective-mass parameters $\gamma_1, \gamma_2, \dots$ are related to those L, M, N, \dots as follows:

$$\begin{aligned} \gamma_1 &= \frac{1}{3}(L + M + N), & \gamma_2 &= \frac{1}{6}(L + M - 2N), & \gamma_3 &= \frac{1}{6}R, \\ \gamma_1' &= \frac{1}{3}(T + 2S), & \gamma_2' &= \frac{1}{6}(T - S), & \gamma_3' &= \frac{1}{6}Q, \\ \eta &= \frac{1}{6}(L - M + R), & \delta &= \frac{1}{6}(L - M - R). \end{aligned} \quad (5)$$

To make the coefficient A of the linear term dimensionless, we introduce $p_0 = \sqrt{2m_0\Delta_c}$.

Taking $|11\rangle, |11\rangle$, and $|1-1\rangle$ as the basic functions, the spin-orbital coupling Hamiltonian is written as¹²

$$H_{so} = \begin{vmatrix} -\lambda & 0 & 0 & 0 & 0 & 0 \\ 0 & 0 & 0 & \sqrt{2}\lambda & 0 & 0 \\ 0 & 0 & \lambda & 0 & -\sqrt{2}\lambda & 0 \\ 0 & \sqrt{2}\lambda & 0 & \lambda & 0 & 0 \\ 0 & 0 & -\sqrt{2}\lambda & 0 & 0 & 0 \\ 0 & 0 & 0 & 0 & 0 & -\lambda \end{vmatrix}, \quad (6)$$

where the first three basic functions correspond to spin up and the second three basic functions correspond to spin down,

$$\lambda = \frac{\hbar^3}{4m_0^2 c^2} \langle X | \frac{\partial V}{\partial x} \frac{\partial}{\partial y} | Y \rangle = \frac{\Delta_{so}}{3}. \quad (7)$$

Δ_{so} is the spin-orbital splitting energy. From the Hamiltonian (6) we obtain the energies of the valence-band top,

$$E = \begin{cases} \frac{1}{2} [(\Delta_c + \lambda) \pm \sqrt{\Delta_c^2 - 2\Delta_c\lambda + 9\lambda^2}] & (\Gamma_7) \\ -\lambda & (\Gamma_9). \end{cases} \quad (8)$$

TABLE II. Effective-mass parameters for hexagonal semiconductors.

| | m_x | m_z | L | M | N | R | S | T | Q | A |
|------|--------|--------|--------|--------|--------|--------|--------|--------|-------|--------|
| CdS | 0.1806 | 0.1788 | 5.0269 | 0.3956 | 0.4789 | 4.6367 | 0.4196 | 5.6767 | 2.000 | 0.8749 |
| CdSe | 0.1756 | 0.1728 | 4.6851 | 0.3389 | 0.3716 | 4.3491 | 0.5719 | 5.3542 | 2.267 | 0.6532 |
| ZnS | 0.2173 | 0.2115 | 4.0784 | 0.3483 | 0.4096 | 3.7352 | 0.3467 | 4.6821 | 1.600 | 0.6629 |

From Eq. (8) and the experimental values of valence-band energies, the parameters Δ_c and λ can be determined.

The eigenenergies and corresponding eigenstates in the quantum spheres are calculated as in Ref. 12. The wave functions are expanded with the spherical Bessel functions and spherical harmonic functions for the zero SOC case,

$$\Psi = \sum_{l,n} \begin{pmatrix} a_{l,n} C_{l,n} j_l(k_n^l r) Y_{l,m-1}(\theta, \phi) \\ b_{l,n} C_{l,n} j_l(k_n^l r) Y_{l,m}(\theta, \phi) \\ d_{l,n} C_{l,n} j_l(k_n^l r) Y_{l,m+1}(\theta, \phi) \end{pmatrix}, \quad (9)$$

where $j_l(x)$ is the spherical Bessel function of l order, $\alpha_n^l = k_n^l R$ is the n th zero point of j_l , R is the radius of the sphere, and $C_{l,n}$ is the normalization constant,

$$C_{l,n} = \frac{\sqrt{2}}{R^{3/2}} \frac{1}{j_{l+1}(\alpha_n^l)}. \quad (10)$$

Because of the hexagonal symmetry, only the z component of the angular momentum M is a good quantum number. The linear terms in the Hamiltonian (3) couple the states of even angular momentum l and odd l ; the summation over l in the expansion of wave function (9) includes both even and odd l , contrary to the case of zinc-blende semiconductors. In that case,¹² the summation over l includes either even l or odd l due to the second-order tensor operators.

In the case of finite SOC, we start from the hole Hamiltonian (3) for both states of spin up and spin down, to which we add the SOC Hamiltonian (6), and keep the z component of the total angular momentum as a constant. For example, if we take $M=0$ in Eq. (9) for the first three basic functions, then we take $M=1$ in Eq. (9) for the second three basic functions, in order that the z component of the total angular momentum is $1/2$.

From Table II we see that the conduction band of the electron is strictly not isotropic, with different effective mass in the z and x, y directions. The effective-mass Hamiltonian of the electron is written as

$$H_e = \frac{1}{2m_x}(p_x^2 + p_y^2) + \frac{1}{2m_z}p_z^2, \quad (11)$$

where m_x and m_z are the effective masses in the x and z directions, respectively. The Hamiltonian (11) can be written as

$$H_e = \frac{p^2}{2m_a} - \frac{1}{2m_b} \sqrt{\frac{2}{3}} P_0^{(2)}, \quad (12)$$

with the effective masses

$$\frac{1}{m_a} = \frac{1}{3} \left(\frac{2}{m_x} + \frac{1}{m_z} \right), \quad (13)$$

$$\frac{1}{m_b} = \frac{1}{3} \left(\frac{1}{m_x} - \frac{1}{m_z} \right). \quad (14)$$

The Hamiltonian (12) couples the states with either even angular momentum l or odd l ; only the z component m is a

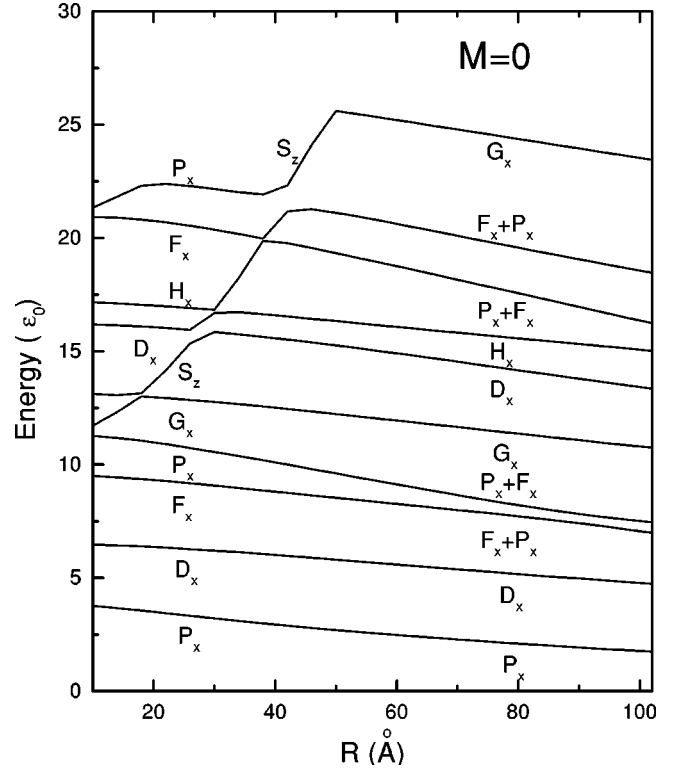


FIG. 1. Energies of hole states ($M=0$) of quantum spheres as functions of sphere radius for the zero SOC case.

good quantum number. From Table II we see that for II-VI compounds the difference between m_x and m_z is so small that we can neglect the coupling between different l states, and consider that l and m are good quantum numbers. The eigenenergy of the electron state $C_{lm} j_l(k_n^l r)$ is

$$E_{lm,n} = \frac{\hbar^2}{2m_a} \left(\frac{\alpha_n^l}{R} \right)^2. \quad (15)$$

III. RESULTS AND DISCUSSIONS

We calculated the energies and wave functions of hole states of CdSe quantum spheres for the zero and finite SOC cases.

(i) *Zero SOC case.* The energies as functions of sphere radius for the z components of angular momentum $M=0,1,2$ are shown in Figs. 1–3, respectively. The symbol of each energy level represents the main component of its wave function. For example, P_x means that the state consists mainly of the $l=1$ state of the effective-mass envelope function multiplied with the X and Y Bloch states of valence-band top.

The unit of energy in Figs. 1–3 is

$$\varepsilon_0 = \frac{\gamma_1}{2m_0} \left(\frac{\hbar}{R} \right)^2. \quad (16)$$

Then we see that the main difference of the energy dependence on the sphere radius R between those of hexagonal and cubic structures is that they are constants for the cubic structure, but are not for the hexagonal structure. This is due to two reasons. The first is the presence of the crystal-field splitting energy between the Γ_6 and Γ_1 energy levels Δ_c ,

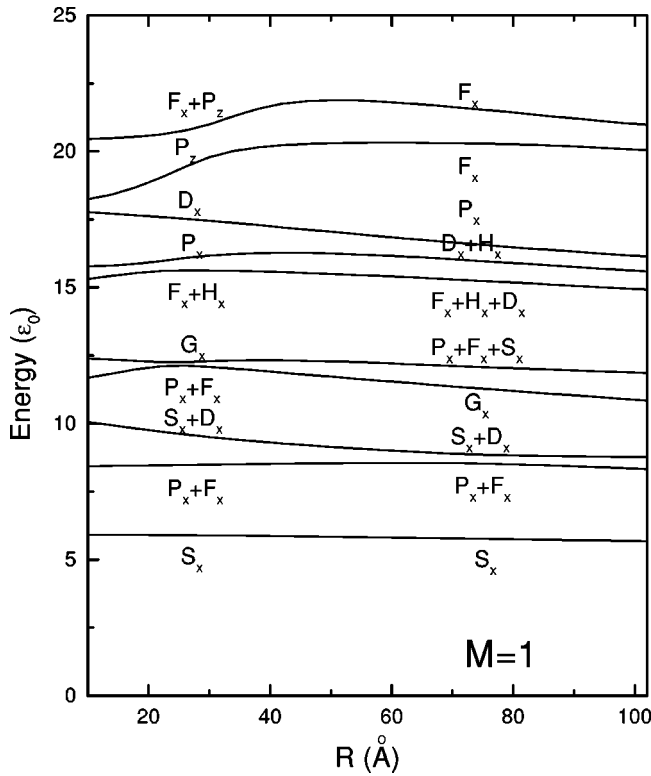


FIG. 2. Energies of hole states ($M=1$) of quantum spheres as functions of sphere radius for the zero SOC case.

which is a constant. Because we take ϵ_0 as units of energy, when the radius R decreases, the energies of quantum energy levels attached to the Γ_1 (Z) state decrease as $\Delta_c R^2$, and intersect or interact with energy levels attached to the

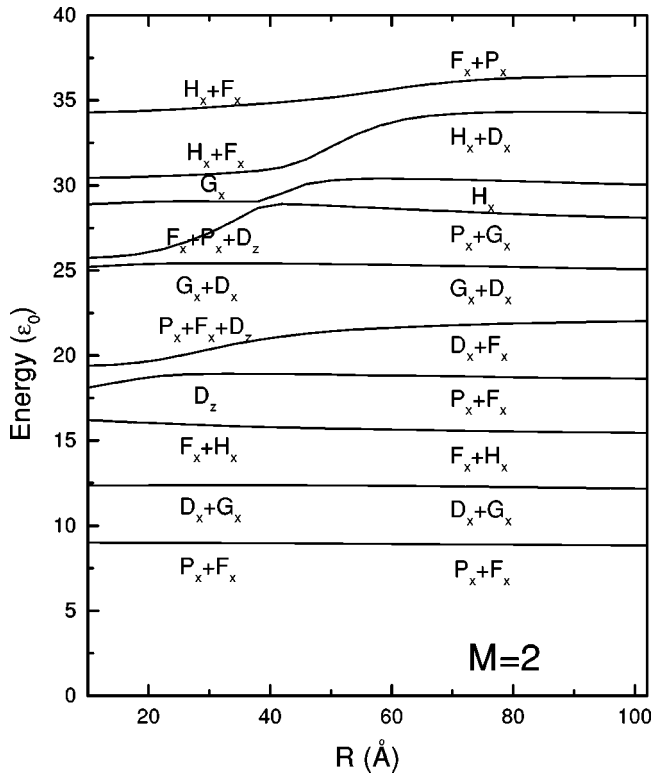


FIG. 3. Energies of hole states ($M=2$) of quantum spheres as functions of sphere radius for the zero SOC case.

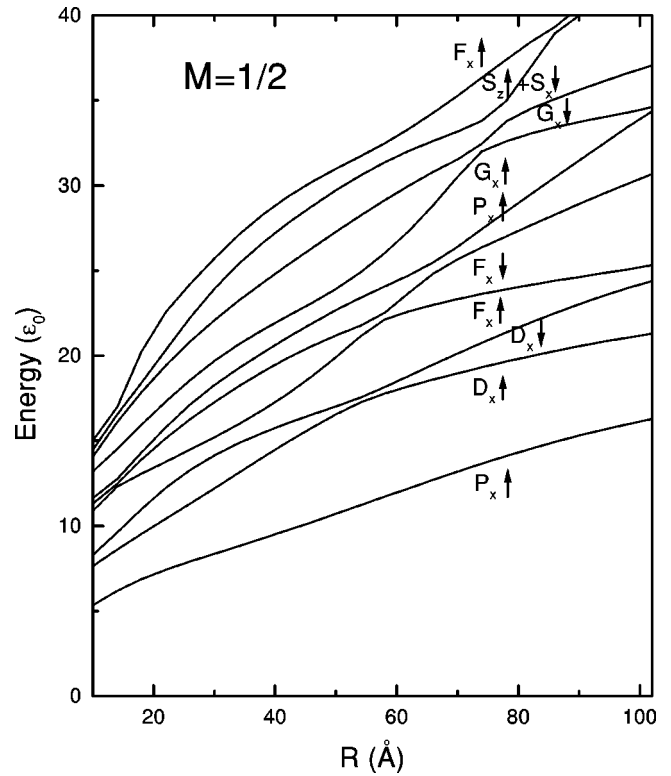


FIG. 4. Energies of hole states ($M=1/2$) of quantum spheres as functions of sphere radius for the finite SOC case.

Γ_6 (X, Y) states. This is apparently shown in Figs. 1 and 3 for the $M=0$ and $M=2$ cases, respectively. The second is the linear terms in the hole Hamiltonian (3). Similarly, if we take ϵ_0 as units of energy, then the linear terms will have a factor R , which increases with R increasing. Due to the interaction of the linear terms, the energy levels decline when R increases, and some wave functions contain mixing of even and odd l states as shown in Figs. 2 and 3. Comparing three figures, we found that the ground state is not the S state (S_x of $M=1$), rather it is the P state (P_x of $M=0$).

(ii) *Finite SOC case.* The actual CdSe has a large spin-orbital splitting energy at the valence-band top ($\Delta_{so} = 0.4$ eV), so we have to consider the finite SOC case. The energies as functions of sphere radius for the z component of angular momentum $M=1/2, 2/3$ are shown in Figs. 4 and 5, respectively. When the radius R increases, the energies of states approach the strong SOC limit. For the case of $M=3/2$ as shown in Fig. 5, the lower several energy levels become flat, varying strictly as $1/R^2$. It is interesting to notice that the hole ground state is not S_x of $M=3/2$ for the radius R smaller than 30 \AA , rather it is P_x of $M=1/2$. This result is in agreement with the “dark exciton” theory proposed recently by Efros *et al.*⁸ The hole S_x state is optically active, while the hole P_x state is optically passive. From our accurate calculation, this is only limited in the range of R smaller than 30 \AA , rather than 50 \AA given in Ref. 8.

The energy difference of S_x and P_x states as functions of the sphere radius R is shown in Fig. 6. When R is larger than 30 \AA , the difference becomes negative, which means that S_x becomes the ground state. This result is in agreement with the experimental results of the resonant Stokes shift.⁸ The

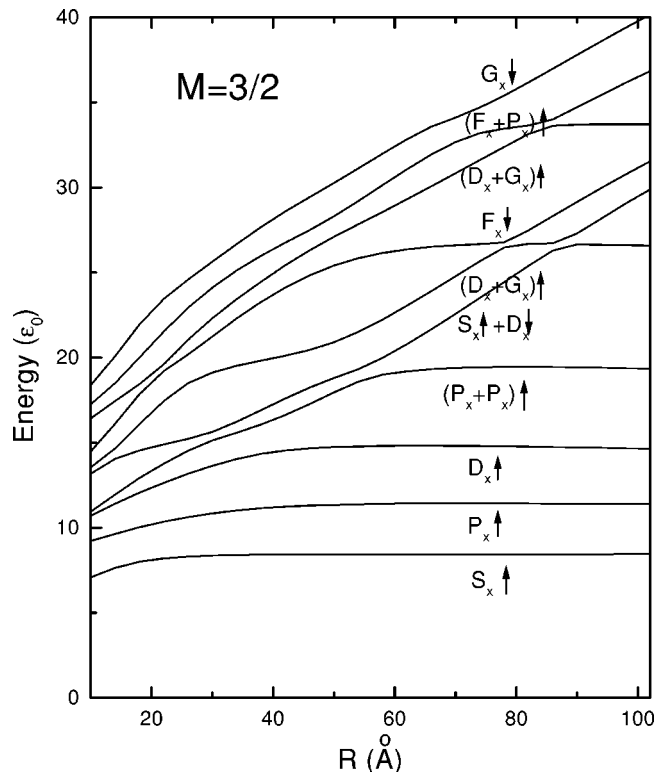


FIG. 5. Energies of hole states ($M=3/2$) of quantum spheres as functions of sphere radius for the finite SOC case.

theoretical absolute values are slightly larger than the experimental values, because we calculated only the band edge energies and we have not taken into account the exciton effect. If we consider the exciton effect, the difference may be smaller.

IV. CONCLUSION

We gave the hole effective-mass Hamiltonian for the semiconductors of wurtzite structure, which is different from those of zinc-blende structure not only in the symmetry, but

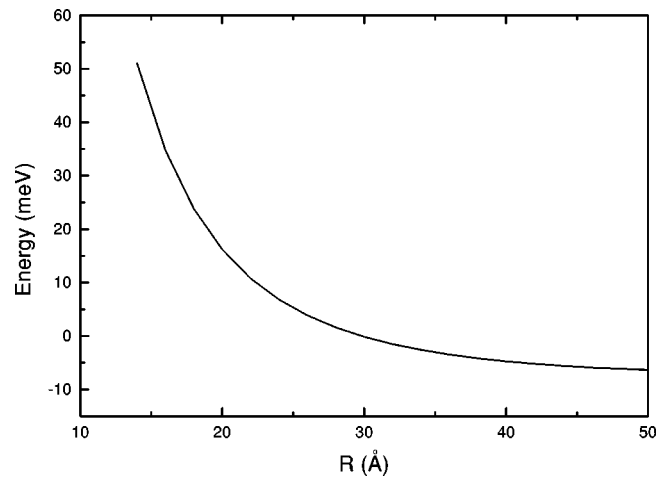


FIG. 6. Energy differences of S_x ($M=3/2$) and P_x ($M=1/2$) states as functions of the sphere radius.

also in the presence of linear terms of the momentum operator. The effective-mass parameters are determined by fitting the valence-band structure near the Γ point with that calculated by the empirical pseudopotential method. The energies and corresponding wave functions are calculated with our effective-mass Hamiltonian for the CdSe quantum spheres. The energies as functions of sphere radius are given for the zero and finite SOC cases. For spheres of cubic structure the energies vary as $1/R^2$, but for spheres of hexagonal structure it is not the case. It is caused by the crystal-field splitting energy between the Γ_6 and Γ_1 energy levels and the linear terms in the Hamiltonian. The ground state is the P_x of the $M=0$ state, not the S_x of the $M=1$ state for the zero SOC case. For the finite SOC case, the ground state is the P_x of $M=1/2$ only for the sphere radius smaller than 30 \AA , in agreement with the experimental results and the ‘‘dark exciton’’ theory.

ACKNOWLEDGMENT

This work was supported by the Chinese National Natural Science Foundation.

¹C. B. Murray, D. J. Norris, and M. G. Bawendi, *J. Am. Chem. Soc.* **11**, 8706 (1993).

²M. A. Hines and P. Guyot-Sionnest, *J. Phys. Chem.* **100**, 468 (1996).

³F. V. Mikulec, B. O. Dabbousi, J. Rodriguez-Viejo, J. R. Heine, H. Mattoussi, K. F. Jensen, and M. G. Bawendi, in *Advances in Microcrystalline and Nanocrystalline Semiconductors—1996*, edited by R. W. Collins, P. M. Fauchet, I. Shimizu, J.-C. Vial, T. Shimada, and P. A. Alivisatos, Materials Research Society Symposia Proceedings No. 452 (MRS, Pittsburgh, 1997), p. 359.

⁴S. A. Empedocles, D. J. Norris, and M. G. Bawendi, in *Advances in Microcrystalline and Nanocrystalline Semiconductors—1996*,

Ref. 3, p. 335.

⁵K. Chang and J. B. Xia, *J. Appl. Phys.* **84**, 1454 (1998).

⁶K. Chang and J. B. Xia, *Phys. Rev. B* **57**, 9780 (1998).

⁷J. B. Xia, *Phys. Rev. B* **40**, 8500 (1989).

⁸Al. L. Efros, M. Rosen, M. Kuno, M. Normal, D. J. Norris, and M. Bawendi, *Phys. Rev. B* **54**, 4843 (1996).

⁹S. L. Chung and C. S. Chang, *Phys. Rev. B* **54**, 2491 (1996).

¹⁰J. B. Xia, K. W. Cheah, X. L. Wang, D. Z. Sun, and M. Y. Kong, *Phys. Rev. B* **59**, 10 119 (1999).

¹¹M. Schlutter, J. R. Chelikowski, S. G. Louie, and M. L. Cohen, *Phys. Rev. B* **12**, 4200 (1975).

¹²J. B. Xia, *J. Lumin.* **70**, 120 (1996).